

Ab initio potential energy surface and anharmonic vibration spectrum of NF_3^+

Yan-Nan Chen(陈艳南), Jiang-Gang Xu(徐建刚), Jiang-Peng Fan(范江鹏), Shuang-Xiong Ma(马双雄), Tian Guo(郭甜), and Yun-Guang Zhang(张云光)

Citation: Chin. Phys. B, 2024, 33 (**1**): 013101. DOI: 10.1088/1674-1056/ad04c6

Journal homepage: http://cpb.iphy.ac.cn; http://iopscience.iop.org/cpb

What follows is a list of articles you may be interested in

Effect of isotope on state-to-state dynamics for reactive collision reactions $O(^3P)+H_2^+ \rightarrow OH^+ + H$ and $O(^3P)+H_2^+ \rightarrow OH + H^+$ in ground state $1^2A''$ and first excited $1^2A'$ potential energy surfaces

Juan Zhao(赵娟), Ting Xu(许婷), Lu-Lu Zhang(张路路), Li-Fei Wang(王立飞)
Chin. Phys. B, 2020, 29 (**2**): 023105. DOI: 10.1088/1674-1056/ab6554

Benchmarking PBE+D3 and SCAN+rVV10 methods using potential energy surfaces generated with MP2+ ΔCCSD(T) calculation

Jie Chen(陈劼), Weiyu Xie(谢炜宇), Kaihang Li(李开航), Shengbai Zhang(张绳百), Yi-Yang Sun(孙宜阳)
Chin. Phys. B, 2020, 29 (**1**): 013102. DOI: 10.1088/1674-1056/ab5fbb

Theoretical investigation of the pressure broadening D_1 and D_2 lines of cesium atoms colliding with ground-state helium atoms

Moussaoui Abdelaziz, Alioua Kamel, Allouche Abdul-rahman, Bouledroua Moncef
Chin. Phys. B, 2019, 28 (**10**): 103103. DOI: 10.1088/1674-1056/ab4043

Density function theoretical study on the complex involved in Th atom-activated C-C bond in C_2H_6

Qing-Qing Wang(王青青), Peng Li(李鹏), Tao Gao(高涛), Hong-Yan Wang(王红艳), Bing-Yun Ao(敖冰云)
Chin. Phys. B, 2016, 25 (**6**): 063102. DOI: 10.1088/1674-1056/25/6/063102

Accurate double many-body expansion potential energy surface of $HS_2(A^2A')$ by scaling the external correlation

Lu-Lu Zhang(张路路), Yu-Zhi Song(宋玉志), Shou-Bao Gao(高守宝), Yuan Zhang(张媛), Qing-Tian Meng(孟庆田)
Chin. Phys. B, 2016, 25 (**5**): 053101. DOI: 10.1088/1674-1056/25/5/053101

Ab initio potential energy surface and anharmonic vibration spectrum of NF_3^+

Yan-Nan Chen(陈艳南), Jian-Gang Xu(徐建刚)†, Jiang-Peng Fan(范江鹏), Shuang-Xiong Ma(马双雄), Tian Guo(郭甜), and Yun-Guang Zhang(张云光)‡

School of Science, Xi'an University of Posts and Telecommunications, Xi'an 710121, *China*

(Received 1 August 2023; revised manuscript received 24 September 2023; accepted manuscript online 19 October 2023)

Potential energy surfaces (PESs), vibrational frequencies, and infrared spectra are calculated for NF_3^+ using *ab initio* calculations, based on UCCSD(T)/cc-pVTZ combined with vibrational configuration interaction (VCI). Based on an iterative algorithm, the surfaces (SURF) program adds automatic points to the lattice representation of the potential function, the one-dimensional and two-dimensional PESs are calculated after reaching a convergence threshold, finally the smooth image of the potential energy surface is fitted. The PESs accurately account for the interaction between the different modes, with the mode q_6 symmetrical stretching vibrations having the greatest effect on the potential energy change of the whole system throughout the potential energy surface shift. The anharmonic frequencies are obtained when the VCI matrix is diagonalized. Fundamental frequencies, overtones, and combination bands of NF_3^+ are calculated, which generate the degenerate phenomenon between their frequencies. Finally, the calculated anharmonic frequency is used to plot the infrared spectra. Modal antisymmetric stretching ν_5 and symmetric stretching ν_6 exhibit a phenomenon of large-intensity borrowing. This study can provide data to support the characterization in the laboratory.

Keywords: *ab initio* methods, potential energy surfaces, vibration frequencies, coupled resonance, infrared spectra

PACS: 31.15.A–, 31.50.Bc, 33.20.Ea, 33.20.Tp **DOI:** 10.1088/1674-1056/ad04c6

1. Introduction

NF_3 is used in the microelectronics industry as a fuel[1] and as an anthropogenic greenhouse gas. Its vibrational levels and molecular spectra have been widely studied.[2–4] However, the vibrational levels and spectra of NF_3^+ received relatively little attention. Initially, the existence of NF_3^+ was questioned, and its potential was studied in terms of the Franck–Condon principle for ionization and dissociation of nitrogen trifluoride by electron impact.[5] Later, it was found to be formed during the synthesis of NF_4^+ salt intermediate by low-temperature UV photolysis. The NF_3^+ radical ion serves as an intermediate during the low-temperature UV photodegradation of the NF_3–F_2–AsF_5 and NF_3–F_2–BF_3 systems, a process that has been successfully observed through experimental electron spin resonance (ESR) spectroscopy.[6] The fragmentation of the valence electronic state of NF_3^+ and its photoelectron spectra were studied using threshold photoelectron-photon coincidence spectroscopy.[7] In the 1980s, there was significant interest in the inversion barrier of NF_3^+. Berkowitz and Greene[8] performed a vibration analysis of the first band of the photoelectron spectrum,[9] revealing the vibrational structure of NF_3^+. *Ab initio* calculations of the NF_3^+ inversion barriers and the inversion vibration dynamics were performed separately.[10,11] The results show that electron correlation is extremely crucial for the inversion barrier. However, its vibration spectrum remains an area of limited research. Molecular vibrational spectroscopy plays an essential role in physicochemical analysis, especially since molecular spectroscopy is an important tool for studying the structure of molecules or ions.[12–14]

In recent years, it is a common phenomenon concerning the use of *ab initio* calculations to predict molecular spectra and vibration frequencies. *Ab initio* calculations[15] have now achieved accurate prediction of a chemical structure and prediction of vibrational frequencies. The potential energy surface[16–19] is one of the most interesting areas in molecular spectroscopy today as it contains information about the dynamics of a molecular framework. Moreover, a number of methods, including vibrational self-consistent fields (VSCF),[20–24] vibrational group state interactions (VCI),[25–28] vibrational Møller–Plesset (VMP),[29,30] vibrational coupled-cluster theory (VCC),[25,31] and second-order perturbation theory (VPT2),[32,33] have been developed in vibrational structure theory (VST). These methods have been applied to the prediction of molecular spectra and vibration frequencies, as the dynamic of the molecular framework directly affects the spectrum. The VSCF/VCI method is widely used in *ab initio* calculation procedures, and the vibration self-consistent field (VSCF) method can strike a balance between accuracy and computation time. The VSCF method was proposed in the late 1970s by many researchers.[34–37] The VCI method[26,38] can make a extremely accurate ap-

†Corresponding author. E-mail: xjgo@xupt.edu.cn
‡Corresponding author. E-mail: zygsr2010@163.com

© 2024 Chinese Physical Society and IOP Publishing Ltd

proach when it appears that a single Hartree product cannot be used to describe a situation, e.g., Ref. [39]. The general VCI calculation procedure is based on the VSCF method.[40–42] Based on the study of VSCF/VCI vibrational wave functions, the spectral intensity can be obtained theoretically by the variational method. For example, the spectra of H_2O,[43,44] CH_4,[44] CH_2O,[6] and C_2H_2[45] have been calculated using the VSCF/VCI method. $(CH_3OH)_2H^+$[46] has been successfully investigated in theoretical calculations using VSCF/VCI. The main objective of this paper is to obtain spectral data for NF_3^+ using more reliable and efficient theoretical algorithms. Therefore, the VSCF/VCI method is selected to study the potential energy surface and vibration spectrum of NF_3^+.

In this paper, we present *ab initio* calculations of the anharmonic frequencies of NF_3^+. Our analysis primarily relies on theoretical calculations, which aim to examine the potential energy surface, anharmonic frequencies, and IR spectrum of NF_3^+. In Section 3 we provide a thorough presentation and analysis of the results obtained from the NF_3^+ calculations. Finally, we present our conclusions in Section 4.

2. Theoretical and computational details

In this paper, the NF_3^+ is calculated from scratch using the Molpro2018 program package.[47] This work aims to construct the *ab initio* potential energy surface of NF_3^+ as accurately as possible by using the latest electronic structure calculations. The generated potential energy surface is employed to perform calculations of the vibrational structure. Afterward, VSCF and VCI calculations are performed to obtain the wave functions corresponding to the vibration states. Finally, the vibrational Schrödinger equation is solved using the wave function to obtain information about the predicted mean vibration geometry and vibration frequency of the NF_3^+ structure.

2.1. Potential energy surface

The balance position, harmonic frequency, and normal mode are calculated before utilizing the VSCF calculation. The SURF program can be used to calculate the potential energy surface (PES) around a reference structure, which is required to determine anharmonic frequencies. Within the surfaces (SURF) program, the PES can be expanded in terms of normal coordinates, the linear combination of normal coordinates, or localized normal coordinates. As a result, it is necessary to perform a harmonic frequency calculation first. Carter *et al.* proposed the n-mode representation (nMR) method.[48–50] Then, the potential can be expressed by a multi-mode expansion,[51] which follows a hierarchical scheme given by

$$V(q_1,\ldots,q_{3N-6}) = \underbrace{\sum_i V_i(q_i)}_{\text{1DCCSD(T)}} + \underbrace{\sum_{i<j} V_{ij}(q_i,q_j)}_{\text{2D:CCSD(T)}} + \underbrace{\sum_{i<j<k} V_{ijk}(q_i,q_j,q_k)}_{\text{3D:CCSD(T)}} + \cdots, \quad (1)$$

with

$$V_i(q_i) = V_i^0(q_i) - V(0), \quad (2)$$

$$V_{ij}(q_i,q_j) = V_{ij}^0(q_i,q_j) - \sum_{r\in\{i,j\}} V_r(q_r) - V(0), \quad (3)$$

$$V_{ijk}(q_i,q_j,q_k) = V_{ijk}^0(q_i,q_j,q_k) - \sum_{\substack{r,s\in\{i,j,k\}\\ r>s}} V_{rs}(q_r,q_s) - \sum_{r\in\{i,j,k\}} V_r(q_r) - V(0), \quad (4)$$

$$V_{ijkl}(q_i,q_j,q_k,q_l) = \cdots, \quad (5)$$

where q_i denotes the coordinates and this expansion needs to be aborted after the n-body contribution. Based on an iterative algorithm, the SURF procedure adds automatic points to the lattice point representation of the potential function, reaching a convergence threshold after iteration. The final calculation results in the PES in different dimensions, which paves the way for subsequent calculations of harmonic frequency.

2.2. Calculation of energy levels

To better understand the molecular vibrations, we used the *ab initio* calculation procedure UCCSD(T) energy gradient analysis to optimize the molecule's equilibrium geometric configuration. Then, we conducted a simple normal mode analysis to determine the vibrational Schrödinger equation in mass-weighted normal mode coordinates:[52]

$$\left[-\frac{1}{2}\sum_{j=1}^{N}\frac{\partial^2}{\partial Q_j^2} + V(Q_1,\ldots,Q_N)\right]\psi_n(Q_1,\ldots,Q_N) = E_n\psi_n(Q_1,\ldots,Q_N), \quad (6)$$

where V is the full potential function for the system, and n is the number of the vibrational normal modes. However, this method does not consider the effect of rotation-vibration coupling. Equation (6) is derived under the VSCF approximation, which is based on the ansatz

$$\psi_n(Q_1,\ldots,Q_N) = \prod_{j=1}^{N}\psi_j^{(n)}(Q_j), \quad (7)$$

which leads to the single-mode VSCF equations

$$\left[-\frac{1}{2}\frac{\partial^2}{\partial Q_j^2} + \overline{V}_j^{(n)}(Q_j)\right]\psi_j^n(Q_j) = \varepsilon_j^{(n)}\psi_j^{(n)}(Q_j), \quad (8)$$

where the effective VSCF potential for mode Q_j is given by

$$\overline{V}_j^{(n)}(Q_j) = \left\langle\prod_{l\neq j}^{N}\psi_l^{(n)}(Q_l)\middle|V(Q_1,\ldots,Q_N)\middle|\prod_{l\neq j}^{N}\psi_l^{(n)}(Q_l)\right\rangle. \quad (9)$$

For the single-mode wave functions, energies and effective potentials must be solved self-consistently. The VSCF approximation for the total energy is then given by

$$E_n^{\mathrm{VSCF}} = \sum_{j=1}^{N} \varepsilon_j^{(n)} - (N-1) \times \left\langle \prod_{l\neq j}^{N} \psi_l^{(n)}(Q_l) \middle| V(Q_1,\ldots,Q_N) \middle| \prod_{l\neq j}^{N} \psi_l^{(n)}(Q_l) \right\rangle. \quad (10)$$

As the VSCF method applies a mean-field approach, correlation effects must be explicitly taken into account in the post-VSCF calculations.[41] Therefore, higher excitation levels are required in the post-VSCF calculations due to the appearance of high-order many-mode operators. As shown in Ref. [41], quadruple excitations cannot be neglected in most applications. The VCSF/VCI method can be used for calculating the non-harmonic frequencies in code multi-mode implementations. The VSCF calculation is first performed to obtain the optimal Hartree product in the vibration state, and here it is used as a reference for the VCI calculation. The excitation below four times the level is included in the VCI calculation (VCISDTQ). For all basis groups included in the VCI matrix, the sum of up to 10 quanta is used. This matrix is diagonalized to obtain the anharmonic frequencies.[46]

3. Results and discussion

3.1. Spectral data for F_2, N_2, NF and fundamental frequency data for NF_3

We employ the UCCSD(T)/cc-pVTZ method to calculate the spectral constants of F_2, N_2, NF, as well as the fundamental frequency of NF_3. Table 1 presents the calculated values for F_2, N_2 and NF, comparing them with the experimental values. For the fundamental frequency of NF_3, the calculated values for the ν_1, ν_2, ν_3, and ν_4 modes are 493.86 cm^{-1}, 648.24 cm^{-1}, 928.34 cm^{-1}, and 1041.42 cm^{-1}, respectively, while the corresponding experimental values[53] are 492 cm^{-1}, 647 cm^{-1}, 907 cm^{-1}, and 1032 cm^{-1}. We can see that the results show excellent agreement with the experiment. Therefore, we further utilized this method for subsequent calculations of NF_3^+.

Table 1. The spectral constants of F_2, N_2, and NF at this benchmark, calculated and compared with the experimental results.

Molecule		R_e (Å)	ω_e (cm^{-1})	$\omega_e\chi_e$ (cm^{-1})	B_e (cm^{-1})	D_e (eV)
F_2	This work	1.4165	917.7443	11.9581	0.8996	1.6312
	Experiment[54]	1.41193	916.64	11.236	0.89091	1.658
N_2	This work	1.1035	2348.5680	13.0274	2.1130	9.6634
	Experiment[54]	1.09768	2358.57	14.324	1.99824	9.90477
NF	This work	1.3185	1149.7326	9.1065	1.2725	3.5126
	Experiment[54]	1.3169	1141.37	8.99	1.2056	3.57048

3.2. Equilibrium geometry of NF_3^+

NF_3^+ is a flat, symmetrical top molecule with spatial geometry. In this work, we employ the spherical harmonic function to perform integration calculations. The spherical harmonic function serves as an eigenfunction of the angular momentum operator. This approach of utilizing spherical harmonic functions for integration lays the foundation for the study of vibrations. NF_3^+ was optimally calculated using UCCSD(T)/cc-pVTZ and its equilibrium geometry parameters were obtained in the process of optimization. The optimized bond lengths $r(N_1–F_2)$, $r(N_1–F_3)$, $r(N_1–F_4)$ are all 1.2839 Å. The key angles $\angle(F_2–N_1–F_3)$, $\angle(F_2–N_1–F_4)$, and $\angle(F_3–N_1–F_4)$ are 113.829°, 113.829°, and 113.83°, respectively. This result is in line with the calculated values in the Comprehensive Computational Chemistry Database (CCCBDB),[55] and so far there are no experimental values for comparison. CCCBDB is a database that provides comprehensive and reliable information on a wide range of molecular properties, energetics, and spectroscopic data. It contains calculated data based on quantum chemical calculations for a large number of molecules.

3.3. Potential energy surfaces

In this work, the one-dimensional (1D) and two-dimensional (2D) PESs of NF_3^+ are derived by using the SURF program in combination with the ploting(PLOT) command. Here q_i represents the trend of the distance to the equilibrium position for each atom in different modes. The change in bond length stretching or compression for each atom in different modes is associated with energy. Since the final mode will remain in the new geometry when it is stationary, this energy is potential energy (position dependent). Figures 1 and S1 in the supporting information are both 1D PESs. The observed 1D PESs of $q_2(A'')$ and $q_6(A'')$ there are symmetric. The symmetry is due to the integrable representation in these two modes that does not fully describe the geometry in the current vibrational state. However, for the four vibration modes of q_1 scissoring, q_3 symmetric deformation, q_4 symmetric, and q_5 asymmetric, the integrability of the symmetry in normal coordinates is expressed as A′, which generates asymmetric 1D PESs, as seen in Fig. S1. Asymmetrical PESs arise because of the tendency of their atoms to change (at a distance from the equilibrium position), with different magnitudes of stretching or compression causing them to generate different potential

energies. In summary, 1D PESs are symmetric when the integrable representation of the vibrational mode is A″, and otherwise, they are asymmetric when the integrable representation is A′.

As shown in Fig. 2, the 2D complete PESs are generated by combining six modes pairwise with each other, two forms of PESs are produced, complete symmetric and axisymmetric. The multi-mode expansion of the PESs is truncated after the 3D contribution, which also contains a 3-mode coupling term. The lowest point in the PESs, when both the horizontal and vertical coordinates tend to zero, is the most stable state of the system, i.e., the equilibrium geometry. Figures 2(a)–2(c) are completely symmetrical due to the complementary orientation of the two modes vibrating against each other in the transverse coordinates of the two modes. Figures 2(d)–2(f) are axisymmetric and arise for reasons related to the q_6 mode. The coupling different vibrational modes has various effects on the variation of the ion potential energy. When the absolute values of the vertical coordinates corresponding to q_i and q_j reach their maximum values at the same time, their mutual coupling leads to the greatest change in potential energy. It is observed that mode q_6 and its different modes coupled to each other produce axisymmetric PESs and that all three sets of couplings have a relatively large effect on the energy of the system. This is due to the ion vibrations that tend to be larger in mode q_6 and therefore have a greater impact on the system when they are coupled to other modes.

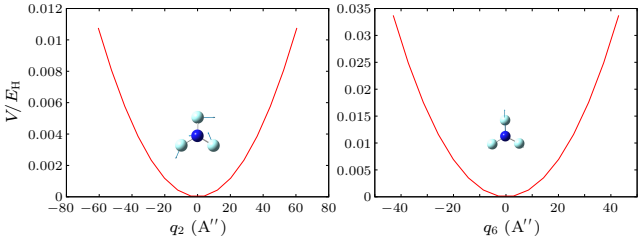


Fig. 1. One-dimensional PESs of molecular vibrations unfolding along q_2(A″) and q_6(A″).

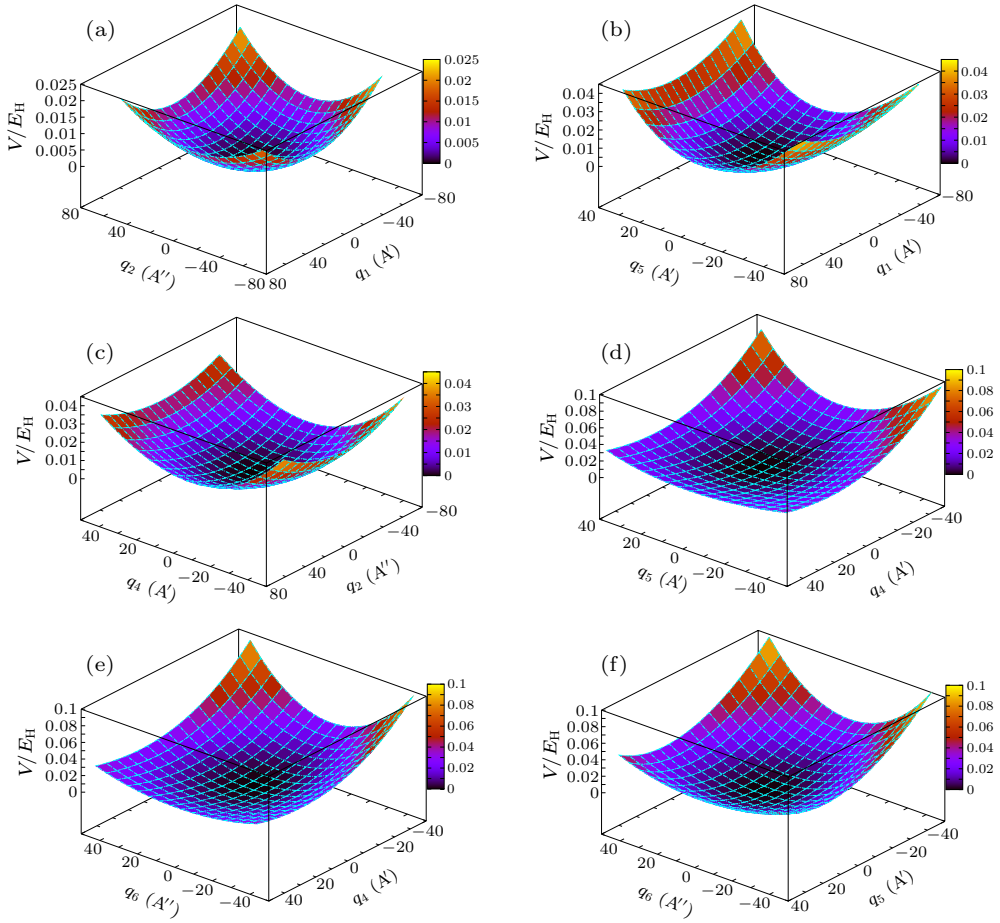


Fig. 2. Two-dimensional complete PESs with different symmetry forms.

The coupling of different modes to each other also generates relative PESs, which are also plotted as shown in Fig. S2 in the supporting information. Looking at Fig. S2, the vertical coordinates of the potential energy appear to be positive and negative, the reason for this is that the zero PES has been chosen as a reference. By using the zero PES as a reference, it is possible to observe more clearly the variation of the potential energy under different modes of coupling. Observation of Figs. S2(a) and S2(b) reveals the same axisymmetric form of the PESs as the complete PESs. Figures S2(a) and S2(b)

are reversed if Fig. S2(a) is assumed to be the front side and Fig. S2(b) is assumed to be the side after reversing it. This phenomenon is caused by the fact that mode q_5 vibrations are in a different direction from mode q_1 vibrations. As shown in Figs. S2(c) and S2(d), the PESs are completely asymmetric and their potential energy tends to change less after coupling in Fig. S2(c). As shown in Figs. S2(c) and S2(d), when the modes have the same integrable representation, e.g., A′ or A″, their mutual coupling produces the completely asymmetric PESs.

In summary, when the PES appears to be symmetrical it saves time and resources for the calculation. The mode q_6 symmetric stretching vibration has the greatest influence on the potential energy change of the whole system. The completely asymmetric PESs are generated when the integrable representations of the modes are identical.

3.4. Vibration frequency

Molecular vibration is a complex phenomenon, in which an actual molecule oscillates through various normal modal motions. Generally, this vibration is a combination of several simple modes. Figures 1 and S1 show that the NF_3^+ molecule has six modes of vibration, including ν_1 in-plane shear vibration, ν_2 in-plane wobble, ν_3 symmetric deformation, ν_4 symmetric stretching, ν_5 antisymmetric stretching, and ν_6 symmetric stretching. The length of the arrows in the diagrams represents the amplitude of the vibrational trend.

Table 2 lists the harmonic vibration frequencies ω_i, anharmonic vibration frequencies ν_i, and anharmonicity correction $\omega_i - \nu_i$ of NF_3^+. Tables 3 and S1 in the supporting information present overtones and combination frequencies, respectively. By observing the fundamental frequencies, we find that the two pairs of vibrational energy levels ν_1 (522.18 cm^{-1}) and ν_2 (522.17 cm^{-1}), ν_5(1249.97 cm^{-1}), and ν_6 (1250.04 cm^{-1}) have a twofold degenerate phenomenon, because the mutual energy band gap between them is less than 1 cm^{-1}. Two of the fundamental frequencies are twofold degenerate and may thus give rise to the Jahn–Teller (JT) effect. Furthermore, we can find a link among mode ν_1, mode ν_2, and mode ν_3 ground states bound to overtones and their combinations, as Table 3 overtones and Table S1 combination bands. Mode $2\nu_1 + \nu_2$ (1567.06 cm^{-1}) is almost equivalent to the sum of the overtones of mode ν_1 and the fundamental frequency of mode ν_2. The same is valid for modes $\nu_1 + 2\nu_2$ (1567.16 cm^{-1}), $2\nu_1 + \nu_3$ (1701.74 cm^{-1}), $2\nu_2 + \nu_3$ (1701.70 cm^{-1}), $\nu_1 + 2\nu_3$ (1832.48 cm^{-1}), $\nu_2 + 2\nu_3$ (1832.45 cm^{-1}), $\nu_1 + \nu_2$ (1044.55 cm^{-1}), $\nu_1 + \nu_3$ (1179.98 cm^{-1}), and $\nu_2 + \nu_3$ (1179.94 cm^{-1}). We also notice that the combination bands resonate with each other in the above-mentioned combinations, e.g., $2\nu_1 + \nu_2$ (1567.06 cm^{-1}) and $\nu_1 + 2\nu_2$ (1567.16 cm^{-1}). Owing to the degenerate phenomenon, we find that mode ν_5 and mode ν_6 also have their combination bands interwound with each other, e.g., $\nu_2 + 2\nu_6$ (3004.51 cm^{-1}) and $\nu_2 + \nu_5 + \nu_6$ (3005.44 cm^{-1}). Therefore, the fundamental frequencies' degenerate phenomenon also leads to this phenomenon between their combined bands.

Table 2. Computed fundamental frequency ν_i (in cm^{-1}), harmonic vibrational wavenumbers ω_i (in cm^{-1}) and anharmonicity corrections $\omega_i - \nu_i$ (in cm^{-1}) of NF_3^+. Here ω_i and ν_i are obtained using the UCCSD(T)/cc-pVTZ method.

Mode	ω_i	ν_i	$\omega_i - \nu_i$
ν_1	529.73	522.18	7.55
ν_2	529.78	522.17	7.61
ν_3	671.60	658.22	13.38
ν_4	1000.25	974.77	25.48
ν_5	1279.42	1249.97	29.45
ν_6	1279.57	1250.04	29.53

Table 3. Computed overtones ν_i (in cm^{-1}), harmonic vibrational wavenumbers ω_i (in cm^{-1}) and anharmonicity corrections $\omega_i - \nu_i$ (in cm^{-1}) of NF_3^+. Here ω_i and ν_i are obtained using the UCCSD(T)/cc-pVTZ method.

Mode	ω_i	ν_i	$\omega_i - \nu_i$
$3\nu_1$	1589.18	1568.64	20.54
$3\nu_2$	1589.33	1568.39	20.94
$3\nu_3$	2014.79	1959.28	55.51
$3\nu_4$	3000.74	2905.41	95.33
$3\nu_5$	3838.26	3708.26	130.00
$3\nu_6$	3838.70	3708.50	130.20
$2\nu_1$	1059.46	1044.56	14.90
$2\nu_2$	1059.55	1044.52	15.03
$2\nu_3$	1343.19	1311.20	31.99
$2\nu_4$	2000.49	1941.82	58.67
$2\nu_5$	2558.84	2481.51	77.33
$2\nu_6$	2559.13	2493.34	65.79

3.5. Vibration spectrum

Molecular spectroscopy is widely used as a "fingerprint of molecules" for the structure of molecules and the chemical composition of substances. The coupled clustering (UCCSD(T)) method in this paper provides accurate predictions of molecular properties and fits the spectral data as shown in Figs. 3 and 4. All the IR absorption peaks in the graph appear in the mid-IR region 400–4000 cm^{-1}. In Fig. 3, the front part of the plot represents the vibrational IR spectrum of NF_3^+ and the back part of the plot represents the vibrational spectrum at 200–1400 cm^{-1} with four distinct peaks, which are marked in the plot with lower case letters. The vibrational spectrum in 200–1400 cm^{-1} represents the absorption peak generated by the fundamental frequency mode. For two different modes whose frequency values are almost close to each other (coupled resonance), intensity borrowing will occur in the vicinity of this frequency. Intensity borrowing is generated at letters a and d in the diagram. The letter d in Fig. 3 indicates the strength borrowed from anti-symmetric stretch ν_5 and symmetric stretch ν_6. It shows a large peak near 1250 cm^{-1} with an intensity of 341.58 km/mol. Similarly, the letter a indicates the intensity borrowed between

the in-plane shear vibration ν_1 and the in-plane wobble ν_2, where the peak is located near 522 cm^{-1} with an intensity of 13.54 km/mol. Symmetric deformation vibration ν_3 and symmetric stretching vibration ν_4 produce peaks of 23.74 km/mol and 15.62 km/mol around 974 cm^{-1} and 658 cm^{-1}, respectively, which are represented in the diagram by the letters b and c, respectively. To facilitate the observation of the remaining weaker overtones and combination bands, IR intensity is plotted in the ranges 1400–2000 cm^{-1} and 2000–3500 cm^{-1}, respectively, as shown in Fig. 4. In combination with the predicted vibration frequencies, it is found that there are vibrationally coupled overtones and combinations of frequencies, which also have intensity borrowing phenomena between them. The peaks at the letters H, N, G, and K in the diagram are intensity borrowed and occur at $\nu_2+\nu_4$ and $\nu_1+\nu_4$, $\nu_2+\nu_6$ and $\nu_1+\nu_5$, $\nu_3+\nu_6$ and $\nu_3+\nu_5$, $\nu_4+\nu_6$ and $\nu_4+\nu_5$, representing intensities of 2.41 km/mol, 0.59 km/mol, 0.34 km/mol, and 9.94 km/mol at 14993 cm^{-1}, 1768 cm^{-1}, 1904 cm^{-1} and 2214 cm^{-1}, respectively. The letters I, M, and L represent the intensities at $\nu_3+\nu_6$, $\nu_5+\nu_2$, and $\nu_5+\nu_6$, which represent intensities of 0.13 km/mol, 0.56 km/mol, and 2.20 km/mol at 1622 cm^{-1}, 1763 cm^{-1}, and 2493 cm^{-1}, respectively.

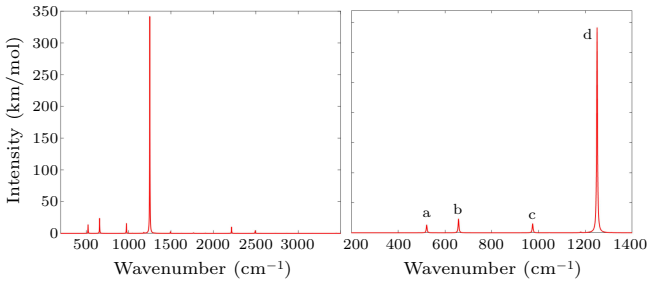


Fig. 3. The infrared spectra produced by the NF_3^+ vibrations and the infrared vibrational spectrum in the range 200–1400 cm^{-1}.

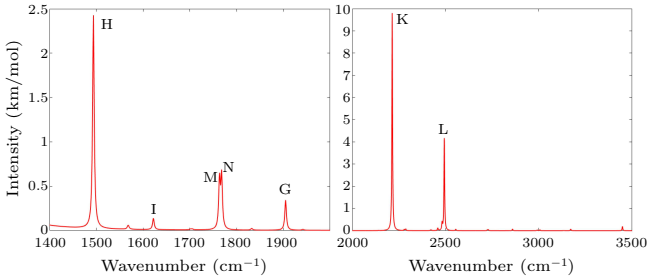


Fig. 4. The infrared vibrational spectra of NF_3^+ in the ranges 1400–2000 cm^{-1} and 2000–3500 cm^{-1}.

4. Summary and conclusion

This paper presents calculations of the PESs, vibrational frequencies, and spectra of NF_3^+ using the UCCSD(T) method in conjunction with the cc-pVTZ basis set within the MOLPRO software package. Highly accurate PESs are fitted to *ab initio* data and constructed with spherical harmonic expansion. Symmetrical potential energy curves are generated in the process of generating 1D PESs when the integrability of the normal transverse coordinate is expressed as A″. Conversely, asymmetric potential curves arise when the integrability is expressed as A′. The coupling of different modes creates 2D relative and complete PESs. The modes coupled to each other have different effects on system potential energy, with mode ν_6 symmetric stretching vibrations having the greatest effect. When irreducible representations of the normal transverse coordinate patterns are all identical, completely asymmetric PESs are created.

In the calculation of the PESs, the Hessian is used to calculate the harmonic frequencies of NF_3^+. In the subsequent calculation of the anharmonic frequencies, the VCI is used to obtain anharmonic corrections for the harmonic frequencies. The fundamental vibrational frequencies of NF_3^+ appear as two pairs of twofold degenerate phenomenon with mutual energy band gaps of less than 1 cm^{-1}, which are out-of-plane shear ν_1 and in-plane oscillation ν_2, respectively, and anti-symmetric ν_5 and symmetric stretching ν_6. Two of them are twofold degenerate and may thus give rise to the Jahn–Teller (JT) effect. This degeneracy is also reflected in the combined and overtone frequencies. Finally, the IR spectrum of the ion is plotted in the mid-infrared region 400–4000 cm^{-1}. Intensity borrowing occurs around this frequency as coupled resonances occur at similar frequencies in different modes, resulting in a shift towards two different modes. Observing the entire spectrum, the greatest intensity in the infrared occurs near the symmetric stretching vibration ν_6. The research in this paper provides data to guide experiments with NF_3^+.

Acknowledgment

Project supported by the National Natural Science Foundation of China (Grant Nos. 52002318 and 22103061).

References

[1] Weiss R F, Mühle J, Salameh P K and Harth C M 2008 *Geophys. Res. Lett.* **35** L20821
[2] Egorov O, Nikitin A, Rey M, Rodina A, Tashkun S and Tyuterev V 2019 *J. Quant. Spectrosc. Radiat. Transfer* **239** 106668
[3] Breidung J, Constantin L, Demaison J, MargulèS L and Thiel W 2003 *Mol. Phys.* **101** 1113
[4] Najib H 2013 *Sci. World* **2013** 813249
[5] Reese R M and Dibeler V H 2004 *J. Chem. Phys.* **24** 1175
[6] Christe K O and Goldberg I B 1978 *Inorg. Chem.* **17** 759
[7] Seccombe D P, Jarvis G K, Fisher B O and Tuckett R P 1999 *Chem. Phys.* **250** 335
[8] Berkowitz J and Greene J 1984 *J. Chem. Phys.* **81** 3383
[9] Curtiss L A 1987 *Chem. Phys. Lett.* **136** 566
[10] Nguyen M T and Ha T K 1986 *Chem. Phys. Lett.* **123** 537
[11] Pouchan C 1985 *Chem. Phys. Lett.* **117** 326
[12] Wilson E B, Decius J C, Cross P C and Sundheim B R 1955 *J. Electrochem. Soc.* **102** 235
[13] Aroca R F 2015 *Structure Elucidation in Organic Chemistry* (Weinheim: Wiley-VCH Verlag) p. 145
[14] Ricardo A 2006 *Surface-Enhanced Vibrational Spectroscopy* (New Jersey: John Wiley & Sons, Ltd) p. 185
[15] Čársky P and Urban M 1980 *Ab Initio Calculations: Methods and Applications in Chemistry* (Berlin: Springer) p. 1
[16] Rauhut G 2004 *J. Chem. Phys.* **121** 9313

[17] Paukku Y, Yang K R, Varga Z and Truhlar D G 2013 *J. Chem. Phys.* **139** 044309
[18] Hrenar T, Werner H J and Rauhut G 2007 *J. Chem. Phys.* **126** 134108
[19] Purvis G D III and Bartlett R J 1982 *J. Chem. Phys.* **76** 1910
[20] Hansen M B, Sparta M, Seidler P, Toffoli D and Christiansen O 2010 *J. Chem. Theory Comput.* **6** 235
[21] Jelski D A, Haley R H and Bowman J M 1996 *Comput. Chem.* **17** 1645
[22] Bowman J M 1986 *Acc. Chem. Res.* **19** 202
[23] Gerber R B and Ratner M A 1988 *Advances in Chemical Physics* (New Jersey: John Wiley & Sons, Ltd) p. 97
[24] Bihary Z, Gerber R B and Apkarian V A 2001 *J. Chem. Phys.* **115** 2695
[25] Carter S, Bowman J M and Handy N C 1998 *Theor. Chem. Acc.* **100** 191
[26] Bowman J M, Christoffel K M and Tobin F 1979 *J. Phys. Chem.* **83** 905
[27] Christoffel K M and Bowman J M 1982 *Chem. Phys. Lett.* **85** 220
[28] Christiansen O 2004 *J. Chem. Phys.* **120** 2149
[29] Christiansen O 2003 *J. Chem. Phys.* **119** 5773
[30] Norris L S, Ratner M A, Roitberg A E and Gerber R B 1996 *J. Chem. Phys.* **105** 11261
[31] Christiansen O 2004 *J. Chem. Phys.* **120** 2140
[32] Barone V 2005 *J. Chem. Phys.* **122** 14108
[33] Barone V, Bloino J, Guido C A and Lipparini F 2010 *Chem. Phys. Lett.* **496** 157
[34] Bowman J M 1978 *J. Chem. Phys.* **68** 608
[35] Gerber R B and Ratner M A 1979 *Chem. Phys. Lett.* **68** 195
[36] Carney G D, Sprandel L L and Kern C W 1978 *Advances in Chemical Physics* (New Jersey: John Wiley & Sons, Ltd) p. 305
[37] Mück-Lichtenfeld C 2003 *Angew. Chem. Int. Ed.* **42** 21
[38] Romanowski H, Bowman J M and Harding L B 1985 *J. Chem. Phys.* **82** 4155
[39] Thompson T C and Truhlar D G 1980 *Chem. Phys. Lett.* **75** 87
[40] Neff M, Hrenar T, Oschetzki D and Rauhut G 2011 *J. Chem. Phys.* **134** 064105
[41] Neff M and Rauhut G 2009 *J. Chem. Phys.* **131** 124129
[42] Rauhut G and Hrenar T 2008 *Chem. Phys.* **346** 160
[43] Carvalho J R and Vidal L N 2022 *J. Comput. Chem.* **43** 1484
[44] Seidler P, Kongsted J and Christiansen O 2007 *J. Phys. Chem. A* **111** 11205
[45] Carvalho J R d 2021 *Estudo do espectro Raman vibracional anarmônico de sistemas moleculares isolados através dos métodos VSCF e VCI* (Ph.D. Dissertation) (Brazil: Universidade Tecnológica Federal do Paraná)
[46] Tan J A and Kuo J L 2018 *J. Chem. Theory Comput.* **14** 6405
[47] Werner H J, Knowles P J, Manby F R, *et al.* 2020 *J. Chem. Phys.* **152** 144107
[48] Carter S and Handy N C 2002 *Chem. Phys. Lett.* **352** 1
[49] Carter S, Bowman J M and Harding L B 1997 *Spectrochim. Acta A* **53** 1179
[50] Carter S and Bowman J M 1998 *J. Chem. Phys.* **108** 4397
[51] Bounouar M 2008 *Theoretical Study of Anharmonic Vibrational Modes and Couplings with the VSCF Algorithm* (Ph.D. Dissertation) (München: Fakultat fur Chemie)
[52] Miller Y, Chaban G M and Gerber R B 2005 *Chem. Phys.* **313** 213
[53] Shimanouchi T 1972 *Tables of molecular vibrational frequencies* (Washington, DC: National Bureau of Standards) Vol. 1 p. 15
[54] Huber K P and Herzberg G 1979 *Molecular spectra and molecular structure: IV Constants of diatomic molecules* (New York: Springer) p. 214
[55] Johnson R D 2006 *NIST computational chemistry comparison and benchmark database* [July 30, 2023] Available at http://srdata.nist.gov/cccbdb